PERGAMON

International Journal of Multiphase Flow 27 (2001) 685–699

International Journal of Multiphase Flow

www.elsevier.com/locate/ijmulflow

Experiments for entrainment rate of droplets in the annular regime ☆

M.A. Lopez de Bertodano [a,*], A. Assad [a], S.G. Beus [b]

[a] *School of Nuclear Engineering, Purdue University, West Lafayette, IN 47907, USA*
[b] *Bettis Atomic Power Laboratory, Westinghouse Electric Corporation, West Mifflin, PA 15122-0079, USA*

Received 23 December 1999; received in revised form 30 July 2000

Abstract

Two-fluid model predictions of film dryout in annular flow are limited by the uncertainties in the entrainment rate of droplets from the liquid film. The main cause of these uncertainties is the lack of separate effects experimental data in the range of the operating conditions in industrial applications.

Air–water and Freon-113 entrainment rate data have been obtained in 10 mm tubes using the double film extraction technique. These experiments have been scaled to approach high-pressure steam–water flow conditions. The effects of surface tension and density ratio, missing from most previous data sets, have been systematically tested.

The entrainment rate mechanism is scaled by the Kelvin–Helmholtz instability at the film surface. Based on this analysis and the new data, a new correlation is proposed that is valid for low-viscosity fluids in small ducts in the ripple-annular regime.

Keywords: Annular flow; Entrainment rate; Atomization; Droplets; Liquid film; Two-fluid model; Film extraction; Freon

1. Introduction

The application of the two-fluid model in annular two-phase flows is limited by the absence of valid constitutive relations. The entrainment rate of droplets from the liquid film is, at present, the greatest uncertainty in the mass balance of the liquid film. The complicated wave structure of the

☆ This is an extended version of a paper that was first presented at ICMF'98 (Lyon, France) and subsequently selected by its Scientific Committee.

* Corresponding author. Tel.: +1-765-494-9169; fax: +1-765-494-9570.
E-mail address: bertodan@ecn.purdue.edu (M.A. Lopez de Bertodano).

0301-9322/01/$ - see front matter
PII: S0301-9322(00)00046-X

film cannot be resolved completely by the state-of-the-art analytical models for waves. The best alternative is to use similarity methods to obtain a semi-empirical correlation based on well-chosen dimensionless numbers. To do this, it is necessary to obtain separate effects data. The entrainment rate data available in the open literature were obtained with air–water experiments at atmospheric conditions. Models based on these data may not be applicable to high-pressure steam–water mixtures.

2. Models

There are several entrainment rate correlations available in the literature. Here, we describe and compare the correlating methods of Dallman et al. (1979) and Kataoka and Ishii (1982) and an analysis based on the Kelvin–Helmholtz instability. Woodmansee and Hanratty (1969) identified by visual observations that the mechanism of entrainment is initiated by the Kelvin–Helmholtz instability.

Dallman et al. (1979) correlated the entrainment rate from a liquid film with the film flow and the gas velocity squared, provided the gas velocity is not too close to the critical velocity for the onset of entrainment and provided that the mass flow rate of the liquid film, $\dot{m}_{\mathrm{LF}}$, is small enough that the dependence of the entrainment rate, $\dot{\varepsilon}$, on $\dot{m}_{\mathrm{LF}}$ is linear

$$\dot{\varepsilon} = k_{\mathrm{A}} \left(\frac{\dot{m}_{\mathrm{LF}} - \dot{m}_{\mathrm{LFC}}}{P} \right) u_{\mathrm{G}}^2 \rho_{\mathrm{G}}^{1/2} \rho_{\mathrm{L}}^{1/2}, \tag{1}$$

where k_{A} is a dimensional coefficient, P the perimeter of the wetted surface and $\dot{m}_{\mathrm{LFC}}$ is the critical liquid mass flow rate required for the onset of entrainment. For air–water upflow, Dykhno and Hanratty (1996) proposed $k_{\mathrm{A}} = 3.8 \times 10^{-6}$ s^2/kg and $\dot{m}_{\mathrm{LFC}}/P = 0.046$ kg/m s.

Kataoka and Ishii (1982) developed a model for entrainment rate based on a force balance at the gas–liquid wavy interface. The final form of Kataoka and Ishii's correlation is defined for two different regimes: under-entrained or developing entrainment, and over-entrained or fully developed entrainment.

The developing entrainment region is defined by

$$\frac{E}{E_\infty} < 1 \quad \text{or} \quad Re_{\mathrm{LF}} > Re_{\mathrm{LF}\infty}, \tag{2}$$

where E is the liquid entrained fraction and

$$E_\infty = \tanh\left(7.25 \times 10^{-7} We_{\mathrm{I}}^{1.25} Re_{\mathrm{L}}^{0.25}\right) \tag{3}$$

is the entrainment fraction correlation for fully developed flow by Ishii and Mishima (1989). Re_{L} is the Reynolds number for the liquid flow flowing alone and

$$We_{\mathrm{I}} \equiv We_{\mathrm{G}} \left(\frac{\Delta\rho}{\rho_{\mathrm{G}}} \right)^{1/3}, \quad We_{\mathrm{G}} = \frac{\rho_{\mathrm{G}} j_{\mathrm{G}}^2 D}{\sigma}. \tag{4}$$

For this region, the entrainment rate is given by

$$\frac{\dot{\varepsilon}D}{\eta_L} = 0.72 \times 10^{-9} Re_L^{1.75} We_I (1 - E_\infty)^{0.25} \left(1 - \frac{E}{E_\infty}\right)^2 + 6.67 \times 10^{-7} \left(Re_L (1 - E)^{0.2} We_I\right)^{0.925} \left(\frac{\eta_G}{\eta_L}\right)^{0.26}. \tag{5}$$

The fully developed and over-entrained regions are defined by

$$\frac{E}{E_\infty} \geqslant 1. \tag{6}$$

For these regions, the entrainment rate becomes

$$\frac{\dot{\varepsilon}D}{\eta_L} = 6.67 \times 10^{-7} \left(Re_L (1 - E)^{0.2} We_I\right)^{0.925} \left(\frac{\eta_G}{\eta_L}\right)^{0.26}. \tag{7}$$

3. Scaling

The model of Taylor (1963) for growth of ripples may be applied to obtain an equation for entrainment rate. The model is based on linear stability theory. Taylor proposed that the perturbations of the surface position, δ, may be modeled as a sum of Fourier components

$$\delta = \delta_0 e^{ikx+\alpha t}, \tag{8}$$

where k is the wave number which is real and the growth coefficient may be a complex number, $\alpha = \mathrm{Im}(\alpha) + \mathrm{R}(\alpha)$. So Eq. (8) may be rewritten as

$$\delta = \delta_0 e^{ikx+\mathrm{Im}(\alpha t)} e^{\mathrm{R}(\alpha t)}. \tag{9}$$

Then, the rate of growth of the ripples is the Lagrangian derivative taken at the wave speed

$$\frac{D_c \delta}{Dt} = \delta_0 e^{ikx+\mathrm{Im}(\alpha t)} e^{\mathrm{R}(\alpha t)} \mathrm{R}(\alpha) = \delta \mathrm{R}(\alpha). \tag{10}$$

The entrainment rate is proportional to the liquid density multiplied by the average growth rate of the ripples

$$\dot{\varepsilon} \propto \rho_L \overline{\delta \mathrm{R}(\alpha)}, \tag{11}$$

where $\bar{\delta}$ is the average height of the ripples. Taylor obtained an analytic solution for the growth rate of capillary waves. When the liquid viscosity is small the asymptotic solution is the same as the Kelvin–Helmholtz inviscid model. The growth rate of the fastest growing waves is

$$\mathrm{R}(\alpha) = 0.384 k_0 u_G \sqrt{\frac{\rho_G}{\rho_L}}, \tag{12}$$

where

$$k_0 = \frac{\rho_G u_G^2}{\sigma} \tag{13}$$

is a wave number associated with the fastest growing waves. For water and Freon-113 Eq. (12) is applicable. However, the coefficient in Eq. (12) is not constant for very viscous fluids, but becomes a function of the liquid viscosity and in such cases, the complete solution obtained by Taylor should be used. The criterion for the low-viscosity range, where Eq. (12) is valid is

$$\frac{\rho_L}{\rho_G}\frac{\sigma^2}{\eta_L^2 u_G^2} > 100. \tag{14}$$

Combining Eqs. (11)–(13), we have

$$\frac{\dot{\varepsilon} D}{\eta_L} \propto \frac{\rho_G u_G^2 D}{\sigma}\frac{\rho_L u_G \bar{\delta}}{\eta_L}\sqrt{\frac{\rho_G}{\rho_L}}. \tag{15}$$

Eq. (15) may be written as

$$\frac{\dot{\varepsilon} D}{\eta_L} \propto We_G Re_{LF}\frac{\bar{\delta}}{h}\frac{u_G}{u_L}\sqrt{\frac{\rho_G}{\rho_L}}, \tag{16}$$

where h is the film thickness. One practical difficulty with Eq. (16) is that the height of the ripples may be quite difficult to measure so it would be hard to validate the effect of $\bar{\delta}/h$. However, Wallis' (1969) correlation for interfacial shear is based on the assumption that the equivalent sand grain roughness is equal to four times the film thickness. So if it is assumed that the amplitude of the ripples is proportional to the sand grain roughness, then $\bar{\delta}/h$ is constant and Eq. (16) may be approximated as

$$\frac{\dot{\varepsilon} D}{\eta_L} \propto We_G Re_{LF}\frac{u_G}{u_L}\sqrt{\frac{\rho_G}{\rho_L}}, \tag{17}$$

where $Re_{LF} = Re_L(1-E)$. This equation is somewhat similar to Eq. (7), the dimensionless correlation proposed by Kataoka and Ishii. It has the same dimensionless groups except for the velocity ratio and the absence of the visosity ratio. The latter is a consequence of the condition given by Eq. (14) and of neglecting viscous effects in the gas phase. There is one more difference, Kataoka and Ishii's correlation is a function of $Re_L(1-E)^{0.2}$ instead of Re_{LF}. Based on the similar dimensionless groups in Eqs. (17) and (7), the following scaling was used to design the experiments:

$$\frac{\dot{\varepsilon} D}{\eta_L} = f\left(Re_L, We_G, \frac{\rho_L}{\rho_G}, \frac{\eta_L}{\eta_G}\right). \tag{18}$$

This scaling is somewhat arbitrary because the velocity ratio is left out. However, neither of the two empirical correlations, Eqs. (1) and (7), support the effect of it. The choice of Re_L vs Re_{LF} was made because both are related by E and Eq. (3). Finally, this should be considered a scaling analysis and not a modeling effort because of well-known deficiencies of the Kelvin–Helmholtz theory for the present case. For example, the observed wavelength of the capillary waves is about 2 orders of magnitude larger than the one derived from Eq. (13). Asali and Hanratty (1993) have proposed a more complete model that considers the effect of shear stresses as well as pressure on the liquid film surface and they have been able to predict the wavelengths within a factor of 2.

Table 1
Annular flow scaling

Fluids	p (MPa)	σ (N/m)	j_L (m/s)	j_G (m/s)	Re_L	We_G	ρ_L/ρ_G	η_L/η_G
Steam–water	13.6	0.0144	0.5	20	2.3×10^4	1.4×10^4	7.5	3.92
Freon-113	2	0.00355	0.357	7.347	2.3×10^4	1.4×10^4	7.1	10.92
Freon-113	1	0.00705	0.426	15.95	2.3×10^4	1.4×10^4	19.3	16.23
Freon-113	0.5	0.01085	0.503	27.49	2.3×10^4	1.4×10^4	40.9	23.65
Air–water	2	0.07275	2.327	84.47	2.3×10^4	1.4×10^4	42.4	52.63
Air–water	1	0.07275	2.327	119.5	2.3×10^4	1.4×10^4	84.7	52.63
Air–water	0.5	0.07275	2.327	168.9	2.3×10^4	1.4×10^4	169.5	52.63

Another important effect that is not presently considered is the observation by Woodmansee and Hanratty (1969) that the capillary ripples atomize from the crests of larger roll waves.

Table 1 shows some scaling calculations based on Eq. (18) for a 10 mm pipe. The reference case is saturated steam–water at 13.6 MPa (i.e., 2000 psia). The free variables of the calculations are the volumetric fluxes. These are adjusted to obtain the same values of Re_L and We_G. Then, the pressure is varied to approach the other two dimensionless numbers. The best result is obtained for saturated Freon at 2 MPa. In this case, the density ratio is very close to the reference and the viscosity ratio is approximately three times larger. At the lowest pressure (0.5 MPa), the density ratio of Freon is five times larger. However, the surface tension in this case is quite close to the reference. For air–water at room temperature, the numbers are not very close and the surface tension is approximately five times larger than the reference.

4. Experiments

4.1. Air–water experiment

The decision was made to build two experiments: an air–water loop and a Freon loop. The main purpose of the air–water loop was to develop the extraction probes and the experimental procedure.

The entrainment rate data for upward annular flow in the air–water experiment have been reported by Lopez de Bertodano et al. (1997). The measurements were obtained using two film extraction probes. The film extraction technique has been developed previously by other researchers (e.g., Cousins and Hewitt, 1968; Sekoguchi et al., 1985).

The test section configuration is shown in Fig. 1. The tube diameter was 9.53 mm and the length to diameter ratio was approximately 440 to ensure fully developed annular flow. The comprehensive measurements included temperature (T), pressure at the injection (p_{in}), pressure in the separator tank (p_{sys}), water flow rate at the injection ($\dot{m}_L$), air flow rate at the injection ($\dot{m}_G$), extracted water flow rate from the first and second extraction units ($\dot{m}_{LF1}, \dot{m}_{LF2}$) and extracted air flow rate from the first and second extraction units ($\dot{m}_{G1}, \dot{m}_{G2}$).

Fig. 2 shows a schematic of the extraction technique. If the liquid film is removed by the first extraction, $\dot{m}_{LF1}$, then the amount of liquid extracted from the second extraction, $\dot{m}_{LF2}$, is the

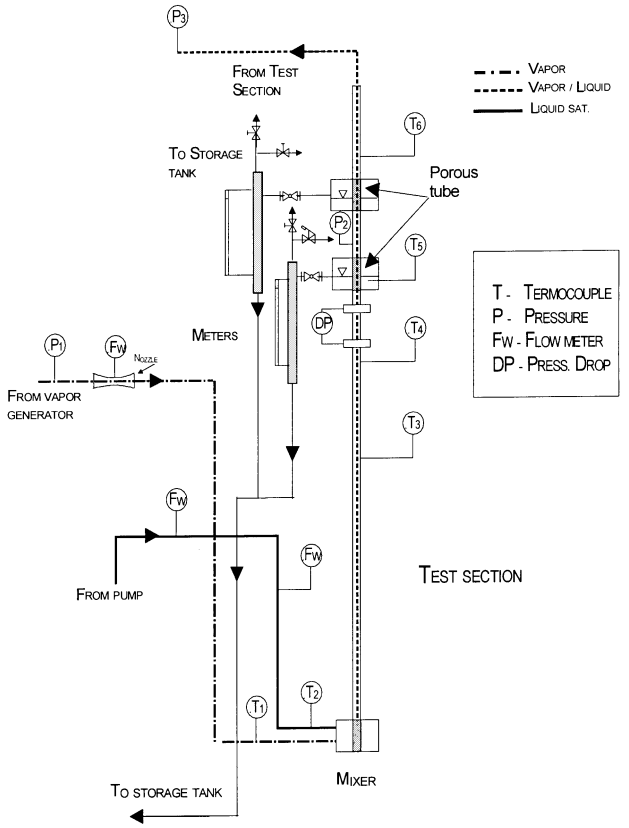

Fig. 1. Test section.

liquid droplet that get deposited along the length L_d, provided that no re-entrainment occurs. For fully developed conditions, it may be assumed that the entrainment rate and the deposition rate are the same just before the first extraction. This technique is reliable for low liquid film flows. Therefore, the present data are limited to the ripple-annular regime. The range of the data is shown in the flow regime map of Hewitt and Roberts (1969) in Fig. 3.

The extraction pore size of 100 μm was selected after comparing measurements with 20, 40, and 100 μm porous tubes. The deposition length, measured from the top of the first extraction unit to the top of second extraction unit, is 0.45 m. To assure proper mating of sections, the acrylic flanges were reamed with a tapered reamer.

The entrainment, E, can be calculated as

$$E = 1 - \frac{\dot{m}_{\mathrm{LF1}}}{\dot{m}_{\mathrm{L}}}. \tag{19}$$

It was found that the liquid film could not be extracted without removing some of the air stream. For low water flow, either visualization or a plot of extracted liquid flow vs extracted air flow can be used to ensure all the liquid flow had been removed. The visual technique worked as follows: when the extracted air flow was increased, the liquid film downstream of the extraction

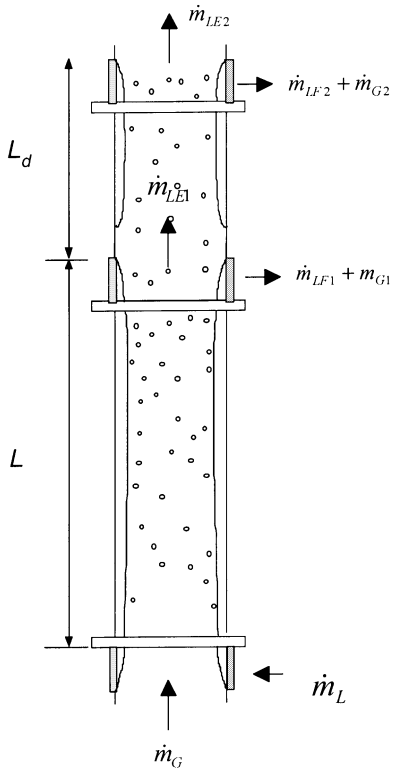

Fig. 2. Double extraction technique.

unit decreased. The extracted air flow was increased gradually, until an abrupt change of the flow regime in the visualization section was observed (i.e., the tube turned from opaque to transparent). After that, no matter how much more air flow was extracted, no difference of the flow regime was observed. It is assumed that the liquid film was extracted completely at that point.

For high water flows, it was hard to tell when the liquid film was extracted completely by visualization. A plot of extracted liquid flow vs extracted air flow was needed to determine when all the liquid film was fully extracted.

The amount of extracted gas was always the minimum necessary to remove the liquid film. On an average, the extracted gas was only 1.5% of the total gas flow. The worst case was 6.3%. Therefore, the error induced by the gas extraction is small.

The deposition rate, $\dot{d}$, and the entrainment rate were calculated from the following equation:

$$\dot{\varepsilon} \cong \dot{d} \cong \frac{\dot{m}_{\mathrm{LF2}}}{\pi D L_{\mathrm{d}}}, \tag{20}$$

where L_{d} is the deposition length shown in Fig. 2.

A set of Cousins and Hewitt's (1968) experimental data were reproduced for testing the performance of the extraction units. The comparison given in Lopez de Bertodano et al. (1997) shows good agreement. The results of an error propagation analysis performed by the same authors are given in Table 2.

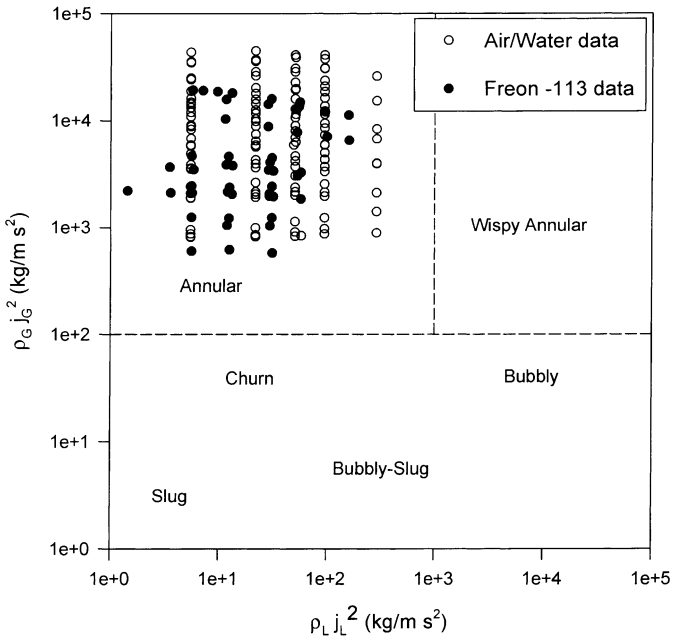

Fig. 3. Data on flow regime map of Hewitt and Roberts (1969).

Table 2
Experimental uncertainties

	$\Delta Re_{LF}/Re_{LF}$	$\Delta We_G/We_G$	$\Delta\dot{\varepsilon}/\dot{\varepsilon}$
Worst case	12.8%	17.3%	13.9%
Average	6.1%	5.0%	2.6%

Another objective of the air–water experiment is to extend the range of the data to higher gas flows and pressures. This was achieved by running very high air flows and by pressurizing the loop. The experimental ranges are listed in Table 3. The high air velocities – up to 126 m/s – are dictated by the scaling analysis. The data are reported in tabulated form by Jan (1996). Further data were obtained at higher liquid flow rates, but the deposition and entrainment rates increase in the wispy-annular regime and re-entrainment occurs between the two extractions so the data are no longer valid.

4.2. Freon experiment

The entrainment rate data of Freon-113 have been reported by Lopez de Bertodano et al. (1998) but the experiment was not described.

In order to scale annular steam–water flow at high pressures and temperatures, Freon has been shown to be one of the best fluids available (Table 1). The adiabatic Freon-113 upward flow test section (Fig. 1) is a 10 mm stainless steel tube with $L/D = 350$. The geometry and the instrument

Table 3
Range of air–water data

Parameter	Unit	Range
Air flow	kg/s	0.0028–0.028
Water flow	kg/s	0.0053–0.038
j_F	m/s	0–0.54
j_G	m/s	10–126
Pressure	kPa	140–660

arrangement are similar to the air–water experiment. However, some additional equipment was required in the Freon experiment:

- The vapor generator tank with 20 kW heaters. This pool boiler generates the vapor that goes into the test section and it is dynamically decoupled from the test section (i.e., one way interaction) to prevent instabilities.
- The liquid feed system with a heater to bring the liquid Freon flowing into the test section up to saturation conditions.
- The bypass loop and condenser. The liquid flow through the bypass loop is approximately 10 times that through the test section. This ensures a constant pressure drop across the test section and eliminates the possibility of instabilities. The vapor exiting the test section mixes with the recirculating liquid at a sparger and the heat is removed through a heat exchanger.
- The pressurizer system, which consists of two tanks, an accumulator tank on top of the loop connected to a large nitrogen tank that maintains the desired pressure.
- A storage tank for long-term Freon storage. This tank also receives the Freon from the extraction units in the test section during the experiment. There is a small pump to transfer the Freon from the storage tank to the rest of the loop before initiation of the experiment.

A small vapor bleed is required to operate the extraction units. The bleed is increased until a "plateau" is obtained in the extracted flow. This procedure is similar to the air–water experiment. However, there are some differences. In that experiment, rotameters were used to measure the bleed gas flows. In the present case, this is impractical so calibrated needle valves are used instead. Since the pressure in the storage tank is well below the pressure in the loop, it is assumed that the flow is choked at the valves. The flows are calculated from a choked flow chart provided by the valve manufacturer.

The geometry of the extraction units and the porous tube specifications are the same as in the air–water loop. However, the operation of the extraction units in the Freon loop requires more care because the condensation of the vapor causes uncertainty in the measurements. The test section and the extraction units were carefully insulated to keep the experiment as close to adiabatic as possible. Before and after each set of data, extraction measurements were collected with no liquid flow to estimate the rate of condensation: the flow in the first extraction is the total condensation in the test section and in the first extraction unit. The amount extracted in the second unit is just the condensation in the second unit. Assuming that the two extractions condense the same amount, the condensation in the test section may be obtained by subtracting the measurement of the second unit from the first. For this procedure to be valid, it is necessary to have no entrainment. Therefore, the vapor flow must be low during this test. If the condensation rate measurements before and after a data set were different, the data set was taken again.

Table 4
Range of Freon-113 data

Parameter	Unit	Range
Gas flow	kg/s	0.0085–0.059
Liquid flow	kg/s	0.0056–0.0365
j_F	m/s	0.05–0.35
j_G	m/s	5.2–25.4
Pressure	kPa	250–500

The range of the present Freon-113 data are listed in Table 4. The data are reported in Appendix A. Further data were obtained at higher liquid flow rates, like in the air–water case, but they were in the wispy-annular regime. Eq. (23) is used to decide when the regime transition occurs.

5. Results

Fig. 4 is a comparison of the current data with the correlation of Dallman et al. (1979). The new air–water data have the same trends of previous data for small pipes. The entrainment rate is proportional to the liquid film flow as shown. It is also proportional to the square of the gas velocity. Also the entrainment rate is proportional to the square root of the gas density since this dependence collapses the data for the four pressures measured. In all these respects, therefore, our data agrees with Dallman et al.'s model. The same may be said for Freon data independently,

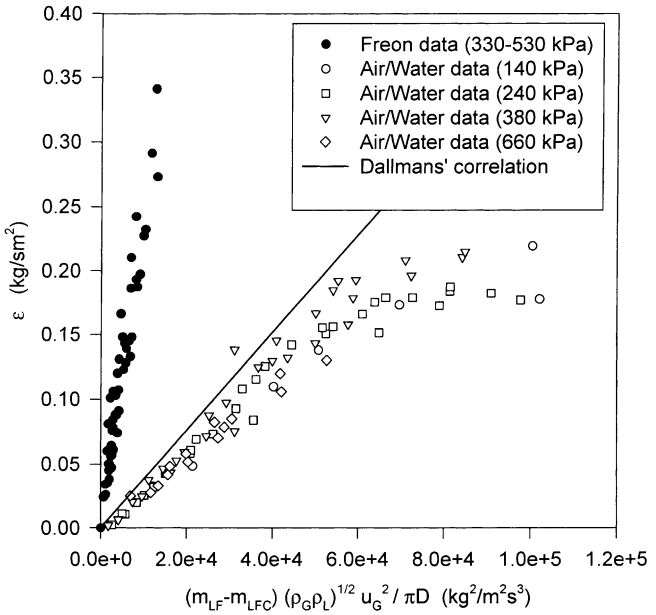

Fig. 4. Comparison with Dallman et al.'s (1979) correlation.

however, they do not collapse with air–water data. The two major differences between the two sets of data are the gas density and the surface tension. However, the air–water data show that the effect of the gas density is properly scaled. Therefore, the surface tension must account for the difference. If the entrainment process is described in terms of the Kelvin–Helmholtz instability, then Eq. (15) indicates that the entrainment rate is inversely proportional to the surface tension. Taking this into consideration collapses the two data sets as shown in Fig. 5. So replacing k_A by k'_A/σ, where k'_A is now dimensionless, Dallman's correlation may account for the effects of density ratio and surface tension

$$\dot{\varepsilon} = k'_A \left(\frac{\dot{m}_{LF} - \dot{m}_{LFC}}{P} \right) \frac{u_G^2 \rho_G^{1/2} \rho_L^{1/2}}{\sigma}. \tag{21}$$

However, for Freon data, $\dot{m}_{LFC}/P = 0.014$ kg/m s was used to obtain a better fit. By simple manipulation this correlation may be written in dimensionless form as

$$\frac{\dot{\varepsilon} D}{\eta_L} = \frac{k'_A}{4} (Re_{LF} - Re_{LFC}) We_G \left(\frac{\rho_L}{\rho_G} \right)^{1/2}. \tag{22}$$

This equation has similarities with (17) but there are some noteworthy differences: the Reynolds number for the onset of entrainment, Re_{LFC}, the absence of the velocity ratio, and the fact that the density ratio is inverted. There are several correlations for Re_{LFC} in the published literature. Using Azzopardi's (1983) correlation for wave inception results in $Re_{LFC} = 80$ for both Freon and water. Fig. 6 shows the plot of the data against Eq. (22). The agreement is good as expected since Fig. 6 is a rearrangement of Fig. 5.

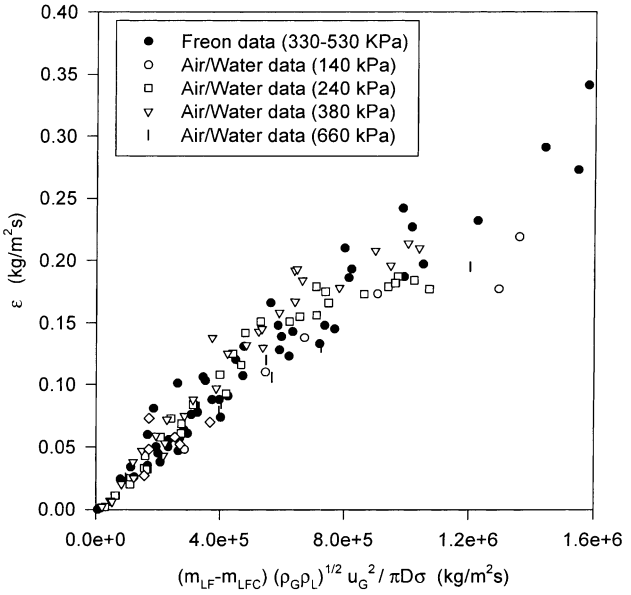

Fig. 5. Comparison with Eq. (21).

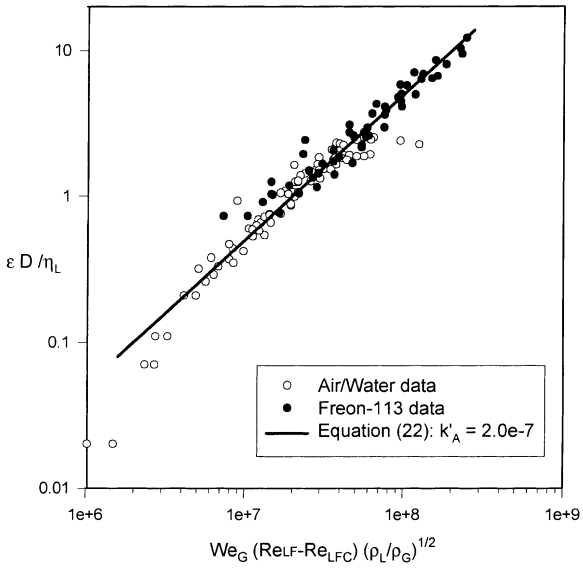

Fig. 6. Comparison with Eq. (22).

Fig. 7 shows the comparison of the entrainment rate correlation of Kataoka and Ishii, Eq. (7), with the data. The proposed dimensionless group $(Re_L(1-E)^{0.2}We_I)^{0.925}(\eta_G/\eta_L)^{0.26}$ collapses air–water data very well for low entrainment rates, but there is some scatter as the entrainment rate becomes larger. Freon data are correlated closer to the air–water data than with Dallman's

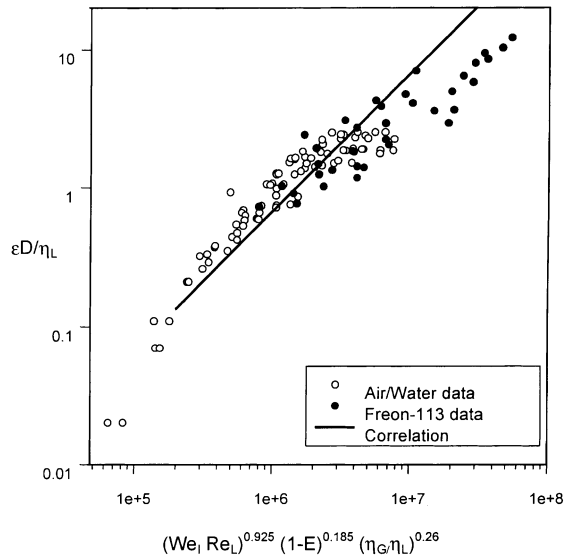

Fig. 7. Comparison with Eq. (7).

correlation. Even though the agreement is not perfect it appears that the surface tension dependence is modeled correctly through the gas Weber number in the same way as Eq. (22). The disagreement between the correlation and the data shown in Fig. 7 occurs when the new data go beyond the original database used to develop the correlation (i.e., low-pressure air–water data at moderate gas flows). The discrepancy arises primarily because the Reynolds number dependence is different from Dallman's correlation or Eq. (22): Kataoka and Ishii's correlation depends on $Re_L(1-E)^{0.2}$, but considering Eqs. (21) and (22) it appears that Re_{LF} is a better choice. Furthermore, the existence of a critical Reynolds number for entrainment was determined experimentally by many researchers (e.g., Dallman et al., 1979; Ishii and Grolmes, 1975) so the Reynolds number dependence should be $Re_{LF} - Re_{LFC}$.

The small dependence of the viscosity ratio in Kataoka and Ishii's correlation is difficult to determine from the present data because it only varies by a factor of 2.

Eq. (22) is only valid in the ripple-annular regime because the deposition and entrainment mechanisms change when the flow becomes wispy-annular and because the film extraction technique does not work properly in this regime so the data cannot support a model. The limit of the extraction data was determined by Helm et al. (1999) as follows:

$$We_G = \frac{18,000}{We_{LF}/Re_{LF}^{0.2}} - 1400, \tag{23}$$

where $We_{LF} = \rho_L j_L^2 D/\sigma$. This equation sets the limit of validity of Eq. (22).

Other limitations of Eq. (22) are:

- The data were obtained in 10 mm tubes, where the entrainment rate varies quadratically with gas velocity. However, the air–water entrainment rate data of Schadel et al. (1990) in 25, 42 and 57 mm tubes showed a linear gas velocity dependence. The effect of the pipe diameter is another aspect of the entrainment rate that is not yet understood.
- Eq. (22) was only tested with low-viscosity liquids so it should not be used for more viscous fluids such as oils that do not satisfy Eq. (14). According to Taylor's theory the growth rate of the ripples is damped by viscosity for highly viscous fluids, so the entrainment rate would be lower. Furthermore, the onset of entrainment may be different too. At present the effect of the liquid viscosity on entrainment rate remains unknown.

6. Conclusion

The objective of this work was to develop a model for the entrainment rate in annular flow within the context of the two-fluid model formulation. Eq. (22) was obtained from two new data sets at conditions beyond what was previously available in the open literature. In particular, the effects of density ratio and surface tension have been systematically tested. The experiments were scaled so that the steam–water conditions existing in boilers and water nuclear reactors would be approached. The new correlation was derived from two previous correlations, Eqs. (1) and (7), and the Kelvin–Helmholtz instability analysis. It combines the strong points of both correlations and the match with previous and present data is satisfactory. It is valid for low-viscosity fluids in small ducts in the ripple-annular flow regime.

Table 5
Freon-113 data

p_{test} (kPa)	$\dot{m}_L$ (kg/s)	$\dot{m}_G$ (kg/s)	ρ_L (kg/m^3)	ρ_G (kg/m^3)	σ (N/m)	E	$\dot{\varepsilon}$ (kg/m^2 s)
334.7	0.0103	0.0131	1392	22.86	0.00984	0.349	0.0497
338.1	0.0104	0.0183	1392	23.07	0.00981	0.481	0.0614
344.9	0.0103	0.0258	1388	23.50	0.00973	0.621	0.0741
338.1	0.0104	0.0093	1390	23.07	0.00981	0.256	0.0342
338.1	0.0069	0.0133	1391	23.07	0.00981	0.370	0.0257
338.1	0.0069	0.0186	1391	23.07	0.00981	0.473	0.0445
338.1	0.0069	0.0256	1387	23.07	0.00981	0.611	0.0465
338.1	0.0069	0.0092	1389	23.07	0.00981	0.184	0.0243
338.1	0.0163	0.0132	1387	23.07	0.00981	0.276	0.1026
344.9	0.0163	0.0186	1386	23.50	0.00973	0.371	0.1283
365.3	0.0163	0.0259	1381	24.79	0.00952	0.573	0.1325
338.1	0.0164	0.0090	1387	23.07	0.00981	0.187	0.0806
467.3	0.0157	0.0141	1349	31.29	0.00857	0.309	0.1013
460.5	0.0157	0.0198	1349	30.85	0.00862	0.405	0.1204
467.3	0.0157	0.0279	1347	31.29	0.00857	0.571	0.1235
474.1	0.0215	0.0514	1344	31.73	0.00851	0.866	0.1858
460.5	0.0216	0.0529	1349	30.85	0.00862	0.846	0.1965
460.5	0.0160	0.0550	1351	30.85	0.00862	0.881	0.1479
446.9	0.0105	0.0577	1352	29.98	0.00874	0.891	0.0777
446.9	0.0090	0.0586	1354	29.98	0.00874	0.881	0.0764
446.9	0.0077	0.0590	1355	29.98	0.00874	0.868	0.0643
443.5	0.0069	0.0593	1355	29.76	0.00877	0.871	0.0504
344.9	0.0222	0.0217	1388	23.50	0.00973	0.422	0.2271
338.1	0.0165	0.0218	1390	23.07	0.00981	0.449	0.1484
338.1	0.0107	0.0231	1393	23.07	0.00981	0.542	0.0911
331.3	0.0071	0.0220	1394	22.65	0.00988	0.511	0.0574
331.3	0.0055	0.0225	1396	22.65	0.00988	0.515	0.0383
324.5	0.0223	0.0158	1396	22.22	0.00996	0.188	0.1934
324.5	0.0166	0.0163	1395	22.22	0.00996	0.245	0.1387
324.5	0.0107	0.0167	1397	22.22	0.00996	0.278	0.0880
324.5	0.0070	0.0169	1396	22.22	0.00996	0.305	0.0559
324.5	0.0056	0.0170	1395	22.22	0.00996	0.370	0.0349
528.6	0.0362	0.0493	1336	35.27	0.00808	0.828	0.3414
521.8	0.0282	0.0508	1336	34.83	0.00813	0.810	0.2909
515.0	0.0208	0.0518	1337	34.38	0.00818	0.827	0.2422
501.4	0.0154	0.0540	1340	33.50	0.00829	0.867	0.1662
487.8	0.0098	0.0563	1343	32.61	0.00840	0.868	0.1060
487.8	0.0365	0.0361	1343	32.61	0.00840	0.720	0.2734
487.8	0.0288	0.0375	1344	32.61	0.00840	0.736	0.2320
481.0	0.0210	0.0392	1345	32.17	0.00845	0.731	0.1872
474.1	0.0154	0.0413	1347	31.73	0.00851	0.740	0.1451
460.5	0.0097	0.0443	1349	30.85	0.00862	0.766	0.1071
446.9	0.0212	0.0236	1355	29.98	0.00874	0.467	0.2101
440.1	0.0155	0.0249	1356	29.54	0.00880	0.488	0.1432
440.1	0.0099	0.0264	1358	29.54	0.00880	0.530	0.0884
419.7	0.0157	0.0185	1361	28.24	0.00898	0.347	0.1310
419.7	0.0100	0.0194	1363	28.24	0.00898	0.365	0.0836
406.1	0.0100	0.0133	1368	27.37	0.00911	0.316	0.0600

Acknowledgements

The authors wish to thank Dr. Mamoru Ishii, who recommended this line of research and Dr. Thomas J. Hanratty, whose timely comment on the importance of surface tension was very helpful. The financial support of Bettis Atomic Power Laboratory is gratefully acknowledged.

Appendix A

See Table 5.

References

Asali, J.C., Hanratty, T.J., 1993. Ripples generated on a liquid film at high velocities. Int. J. Multiphase Flow 19, 229–243.

Azzopardi, B.J., 1983. Mechanisms of entrianment in annular two-phase flow. UKAEA Report AERE-11068.

Cousins, L.B., Hewitt, G.F., 1968. Liquid phase mass transfer in annular two phase flow: droplet deposition and liquid entrainment. UKAEA Report AERE R5657.

Dallman, J.C., Jones, B.G., Hanratty, T.J., 1979. Interpretation of Entrainment Measurements in Annular Gas–Liquid Flows. Two-Phase Momentum, Heat and Mass Transfer in Chemical, Process and Energy Engineering System, vol. 2, Hemisphere, Washington, DC, pp. 681–693.

Dykhno, L.A., Hanratty, T.J., 1996. Use of the interchange model to predict entrainment in vertical annular flow. Chem. Eng. Comm. 141–142, 207–235.

Helm, D.E., Lopez de Bertodano, M., Beus, S.G., 1999. The limit of the film extraction technique for annular two-phase flow in a small tube. 33rd National Heat Transfer Conference, Albuquerque, New Mexico, August, pp. 15–17.

Hewitt, G.F., Roberts, D.N., 1969. Studies of two-phase flow patterns by simultaneous X-ray and flash photography. UKAEA Report AERE-M 2159.

Ishii, M., Grolmes, M.A., 1975. Inception criteria for droplet entrainment in two-phase concurrent film flow. AIChE J. 21, 308–318.

Ishii, M., Mishima, K., 1989. Droplet entrainment correlation in annular two-phase flow. Int. J. Heat Mass Transfer 32, 1835–1846.

Jan, C.S., 1996. Annular air–water flow entrainment experiment in a vertical pipe. M.S. thesis, Purdue University, West Lafayette, IN, USA.

Kataoka, I., Ishii, M., 1982. Mechanism and correlation of droplet entrainment and deposition in annular two-phase flow. NUREG/CR-2885, ANL-82-44.

Lopez de Bertodano, M.A., Jan, C.S., Beus, S., 1997. Annular flow entrainment rate experiment in a vertical pipe. Nucl. Eng. Design 178, 61–70.

Lopez de Bertodano, M.A., Assad, A., Beus, S., 1998. Entrainment rate of droplets in the ripple annular regime for small vertical ducts. Nucl. Sci. Eng. 129, 72.

Schadel, S.A., Leman, G.W., Binder, J.L., Hanratty, T.J., 1990. Rate of atomization and deposition in vertical annular flow. Int. J. Multiphase Flow 16, 363–374.

Sekoguchi, K., Tanaka, O., Ueno, T., 1985. On the determination method of entrained droplet flow rate in the disturbance wave region of annular flow. Bull. JSME 28, 1105–1112.

Taylor, G.I., 1963. Generation of Ripples by Wind Blowing over a Viscous Fluid. The Scientific papers of Sir Geoffrey Ingram Taylor 3, Cambridge University Press, pp. 244–254 (Chapter 25).

Wallis, G.B., 1969. One-dimensional Two Phase Flow. McGraw-Hill, New York.

Woodmansee, D.E., Hanratty, T.J., 1969. Mechanism for the removal of droplets from a liquid surface by a parallel air flow. Chem. Eng. Sci. 24, 299–307.